ANALYSIS OF FUNCTIONAL MAGNETIC RESONANCE IMAGES BY WAVELET DECOMPOSITION

Urs E. Ruttimann, Nick F. Ramsey*, Daniel W. Hommer*, Philippe Thévenaz**, Chulhee Lee**, Michael Unser***

* Section on Brain Electrophysiology and Imaging, National Institute on Alcohol Abuse and Alcoholism; ** Biomedical Engineering and Instrumentation Program, National Center for Research Resources

National Institutes of Health, Bethesda, Maryland 20892, USA

ABSTRACT

The use of the wavelet transform to detect differences between sequentially acquired functional magnetic resonance images (fMRIs) is explored. A statistical data model is developed that makes use of the orthogonality and regularity conditions of the wavelets to achieve a signal decomposition into uncorrelated components, enabling application of standard parametric tests of significance on wavelet coefficients directly. This overcomes the problems associated with high intervoxel correlations in the spatial domain, and achieves economy in statistical testing by limiting the search for significant signal components to a subspace where the signal power is located. Thus, a smaller p-value adjustment for multiple testing is required, resulting in a lower detection threshold for a given overall level of statistical significance. For the fMRIs investigated, a 10:1 reduction in the number of statistical tests was achieved, and about 1% of the wavelet coefficients were significant ($p<0.05$ per volume), which then served to resynthesize the difference images by inverse wavelet transform.

1. INTRODUCTION

Functional neuroimaging is a fast evolving area aimed at measuring brain activity during task performance. Functional magnetic resonance imaging (fMRI) is only the most recently developed modality [1], which distinguishes itself from earlier methods (e.g. PET, SPECT) in that no exposure to ionizing radiation is involved, better spatial and temporal resolution is achieved, and a relatively straightforward co-registration to anatomical MRIs acquired on the same machine can be attained. The latter feature greatly facilitates the pursuit of one of the major goals in neuroscience, the association of structure with function.

Functional imaging, as opposed to the more familiar static or anatomical imaging used for mapping brain structure, provides information on physiological processes in the brain of awake human beings while they are performing controlled perceptual or cognitive tasks. Of interest is usually the detection of differences in focal neuronal activation patterns, either between different groups of subjects (e.g. normal versus diseased) or between controlled experimental conditions within the same subject (e.g. at rest versus solving a word puzzle). A shortcoming of fMRI is that only the hemodynamic consequences of brain activity are assessed rather than a more proximate measure of neuronal activity. The method is based on the fact that hemoglobin becomes highly paramagnetic in its deoxygenated state, which introduces local magnetic field inhomogeneities that extend well into the extravascular space. These inhomogeneities result in a local dephasing of the proton-spins that weakens the MR signal (T2* effect). Upon brain activation, the local hemodynamic response overshoots the blood flow requirement for sustaining the increased metabolic demand. This results in a net increase of the venous blood oxygenation level, reducing the local field inhomogeneities and thus, producing an increase in the MR signal.

The natural variability in the resulting 2-D or 3-D brain activity maps is large and complex, requiring the support of statistical methods for the detection of signal differences that range typically from 2% to 8% on conventional 1.5 Tesla machines. The problem of poor signal-to-noise ratio (SNR) conditions is further exacerbated in that, for the spatial localization desired for meaningful neurophysiological interpretation of the data, the number of voxels investigators wish to examine, is typically very large. In engineering terms: both the spatial location and the spatial extent (or equivalently the spatial-frequency bandwidth) of the signal to be detected are unknown.

Signal detection by statistical testing of individual voxels is problematic without the use of a rigorous data model because of the potentially large number of tests to be performed, and the difficulty of assigning proper significance levels due to substantial intervoxel correlation. Some alleviation to these problems is proposed in this paper. We employ a discrete wavelet transform to attain an orthogonal decomposition of the functional images with respect to spatial location and resolution bandwidth. The good localization properties of the wavelets in both the spatial and the frequency domains can then be used to take advantage of the better SNR conditions at lower image resolutions, and to develop statistical models that enable the application of standard parametric tests of significance on wavelet coefficients directly. Due to orthogonality and regularity conditions imposed on the wavelet basis, these tests are unhampered by the intervoxel correlations existing in the spatial domain .

2. METHODS

2.1. Image Acquisition

Images were obtained using a clinical 1.5 Tesla scanner (SIGNA, General Electric, Milwaukee) with standard quadrature head coil. Both structural and functional images were acquired from the same region of the brain. For anatomical detail, inversion recovery images (TI/TR 800/3000 msec) were obtained that matched the functional images in location, orientation (45° relative to the AC-PC line) and thickness (3 mm + 1 mm gap), yielding a data matrix of 15 slices with 256x128 pixels over a field of view (FOV) of 240 mm. For the functional scans, an Echo-Shifted FLASH sequence was used (TE/TR 29.1/20 ms, flip angle 11°, FOV 64 mm, data matrix 16 slices of 64x64 pixels) [2]. The entire volume was acquired within 20 s. Uniformity limitations of the RF field excitation restricted the image analysis to the 10 innermost slices, covering a 40 mm section with 4 mm

0-8186-7310-9/95 $4.00 © 1995 IEEE

thick contiguous slices of nominal in-plane resolution of 3.75x3.75 mm. Pilot experiments determined that the extent of local field inhomogeneity effects caused by the nasal cavity (air/tissue susceptibility difference) was minimized at the chosen slice orientation of 45°.

A multivalve olfactory stimulation system was built from nonmagnetic material (teflon and brass) that permitted to connect small vessels containing different odors (Coconut or Muguet, International Flavors and Fragrances, Union Beach, NJ) to a nasal cannula. An air pump located outside the scanner room supplied a continuous stream of filtered air, which could either be led directly to the nasal cannula (control condition) or diverted first through one of the odor containers (olfactory stimulation). A stimulation cycle consisted of 2 consecutive 20 s functional scans, with a 7 s interval between the scans. Olfactory stimulation was switched on at the end of the first scan, and off at the end of the second scan. For each subject 8 cycles were acquired, spaced 3 minutes apart to allow for washing out of the odors from the valve system and nasal cavity. To minimize motion artifacts, all subsequent fMRI scans were digitally registered to the first scan (3-D translation and rotation) by a procedure that minimized the squared gray-level difference over all intracranial voxels. The Marquardt-Levenberg algorithm was used in a coarse-to-fine strategy to estimate the optimal transformation parameters from cubic-spline resolution pyramid representations of the volumes to be registered [3].

2.2. Statistical Analysis

For the data analysis, registered slices obtained during olfactory stimulation were subtracted from the corresponding baseline slices of each stimulation cycle, i, yielding $N = 8$ difference images, $f_i(s,t)$. These images are assumed to be represented by the population model

$$f_i(s,t) = \mu(s,t) + e_i(s,t), \quad i = 1, ..., N, \tag{2.1}$$

where $\mu(s,t)$ represents the underlying (deterministic) spatial pattern to be detected, and e is a Gaussian random field with $E[e] = 0$ and $E[e(s,t)\, e(s',t')] = \sigma^2 \delta(s-s', t-t')$. To estimate $\mu(s,t)$, averaging over the N replications is performed, yielding

$$\hat{\mu}(s,t) = \frac{1}{N} \sum_{i=1}^{N} f_i(s,t) \ , \tag{2.2}$$

$$\tilde{\sigma}^2(s,t) = \frac{1}{N-1} \sum_{i=1}^{N} \left[f_i(s,t) - \hat{\mu}(s,t) \right]^2 \ , \tag{2.3}$$

which satisfies

$$E[\hat{\mu}(s,t)] = \mu(s,t) \ , \text{ and } \mathrm{Var}[\hat{\mu}(s,t)] = \sigma^2/N \ . \tag{2.4}$$

By pooling $\tilde{\sigma}^2(s,t)$ over all intracranial *(IC)* pixels, n_{pix}, an estimate of σ^2 with a large number of degrees of freedom is obtained, which is assumed to be fixed and a good approximation of σ^2:

$$\tilde{\sigma}^2 = \frac{1}{n_{pix}} \sum_{s,t \in IC} \tilde{\sigma}^2(s,t) \approx \sigma^2 \ , \ n_{pix} = \#IC \ . \tag{2.5}$$

The orthogonal spline (or Battle-Lemarié) wavelets were used as the bases for the wavelet transform. This family provides symmetric wavelet functions, whose regularity can be conveniently controlled by specifying the polynomial order of the spline. We investigated, the suitability of splines of orders 0 (Haar basis), 1, 3, and 5, and selected cubic splines for presentation of the results. The digital implementation of the wavelet transform followed the filterbank algorithm of Mallat [4, 5], and extension to two dimensions was achieved by the tensor product representation

$$\begin{aligned} \Psi_j^1(m,n) &= 2^{-j} \varphi(2^{-j}x - n)\, \psi(2^{-j}y - m) \ , \\ \Psi_j^2(m,n) &= 2^{-j} \psi(2^{-j}x - n)\, \varphi(2^{-j}y - m) \ , \\ \Psi_j^3(m,n) &= 2^{-j} \psi(2^{-j}x - n)\, \psi(2^{-j}y - m) \ , \ m,n \in \mathbf{Z} \end{aligned} \tag{2.6}$$

defining an orthonormal basis associated with the two-dimensional scaling function

$$\Phi_j(m,n) = 2^{-j} \varphi(2^{-j}x - n)\, \varphi(2^{-j}y - m) \ , \ m,n \in \mathbf{Z} \ . \tag{2.7}$$

Using these bases, the average difference image can be decomposed as

$$\hat{\mu}(s,t) = \sum_{m,n \in \mathbf{Z}} \hat{c}_J(m,n) \Phi_J(m,n) + \sum_{j=1}^{J} \sum_{k=1}^{3} \sum_{m,n \in \mathbf{Z}} \tilde{d}_j^k(m,n)\, \Psi_j^k(m,n), \tag{2.8}$$

where the coefficients $\hat{c}_J(m,n)$ represent the approximation image at resolution level J, and $\tilde{d}_j^k(m,n)$ are the wavelet coefficients at resolution level j, providing horizontally, vertically and diagonally oriented image detail (k=1,2,3, respectively). The approximation and wavelet coefficients are the projections (inner products) of $\hat{\mu}(s,t)$ onto the corresponding orthogonal resolution spaces

$$\hat{c}_J(m,n) = \left\langle \hat{\mu}(s,t), \Phi_J(m,n) \right\rangle \ , \ m,n \in \mathbf{Z} \ , \tag{2.9}$$

$$\tilde{d}_j^k(m,n) = \left\langle \hat{\mu}(s,t), \Psi_j^k(m,n) \right\rangle \ , \ m,n \in \mathbf{Z}, \ j = 1, ..., J, \ k = 1,2,3 \ . \tag{2.10}$$

Under the null hypothesis H_0: $\mu(s,t) = 0$. Substituting (2.4) into (2.9) and (2.10), and using the orthogonality of the bases, it follows that

$$\hat{c}_J(m,n)/\sigma_N \sim N(0,1) \ , \ \tilde{d}_j^k(m,n)/\sigma_N \sim N(0,1) \tag{2.11}$$

$$\sum_{m,n \in IC_J} \left[\hat{c}_J(m,n)/\sigma_N \right]^2 \sim \chi^2_{n_J} \ , \text{ and} \tag{2.12}$$

$$\sum_{m,n \in IC_j} \left[\tilde{d}_j^k(m,n)/\sigma_N \right]^2 \sim \chi^2_{n_j} \ , \ j = 1, ..., J, \ k = 1,2,3 \ , \tag{2.13}$$

where $\sigma_N^2 = \sigma^2/N$, and $n_j = \#IC_j$ is the number of intracranial pixels at resolution level j. Hence, (2.13) enables testing H_0 by $3*J$ chi-square tests, examining whether all wavelet coefficients $\tilde{d}_j^k$ in a particular channel (resolution j and orientation k) are jointly zero.

By assigning to each of these chi-square tests a significance level $\alpha = p/(3*J*10)$ (Bonferroni correction for the 10 slices in this experiment), the overall significance per volume was maintained at the specified level p=0.05. All coefficients in a channel passing the chi-square tests were set to zero. Those in significant

channels were subjected individually to follow-up z-tests based on (2.11), and retained only if significant at a level adjusted for the total number of tests performed in these remaining channels. Application of the inverse wavelet transform to this reduced set of coefficients yielded the reconstruction of the desired signal difference image.

3. RESULTS

Fig. 1 (a) shows one of the difference images for a center slice of the sampled volume, and Fig. 1 (b) presents the result after averaging according to (2.2). The cubic spline wavelet coefficients of this average image for J=4 levels are displayed in Fig. 1 (c). Statistical testing produced 12 significant coefficients (overall $p<0.05$), displayed in Fig. 1 (d).

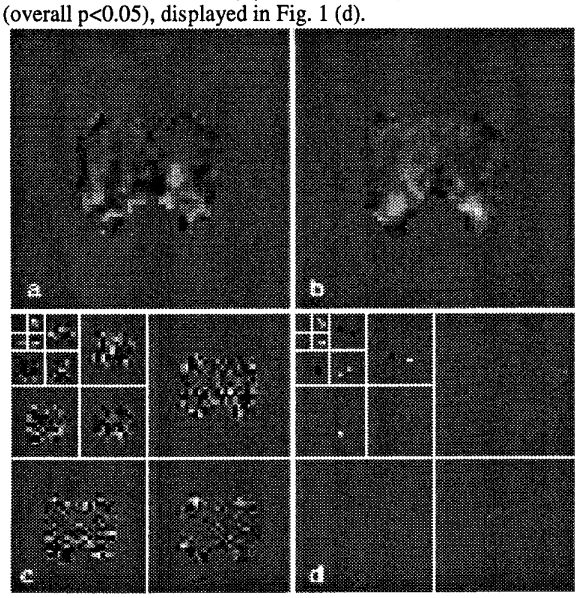

Fig.1 (a) fMRI difference image between olfactory stimulus on and off; (b) average difference image of 8 stimulation cycles; (c) wavelet decomposition with cubic splines; (d) significant ($p<0.05$) wavelet coefficients.

Application of chi-square testing according to (2.13) to the 10 slices encompassing 7001 intracranial voxels, resulted in total search space reductions of 88.2%, 88.2%, 90.0%, and 90.1%, for spline wavelets of orders 0, 1, 3, and 5, respectively. Hence, the p-level for individual tests (Bonferroni adjustment) was reduced by about a factor of 10 compared to voxel-based testing, which itself is difficult to interpret due to spatial correlation. The corresponding number of significant ($p<0.05$) wavelets determined by the follow-up z-tests (2.11) were 95 (1.36%), 77 (1.10%), 76 (1.09%), and 68 (0.97%), respectively. The slightly larger number of significant coefficients for the lower-order splines is due to their diminished capacity to suppress cross-correlation between different resolution channels [6].

Fig. 2 shows for the same slice the original difference image (a), and the reconstructed difference images (b-d) obtained by applying the inverse wavelet transform to the reduced set of significant coefficients. Since most of the deleted coefficients were located in higher resolution channels, a significant amount of noise reduction was achieved, while the main features of the signal were retained. The reconstruction based on Haar wavelets (Fig. 2 b) is perhaps too "blocky" to be of practical use, however, it does provide a valid, cursory abstraction of the main regions of signal change. Both reconstructions employing higher-order wavelets provide reasonable representations of the main focal changes, and there is little visual difference between the results based on first- (c) and third-order (d) wavelets.

Fig. 3 shows 6 contiguous anatomical MRI slices from one subject (anteroposterior direction from top left to bottom right), over which regions of significant functional signal change >1% are superimposed (increase - white, decrease - black). Signal increases are demonstrated over the posterior orbitofrontal and pyriform cortices (anterior slices), and over the amygdaloid nuclei, all areas associated with the processing of olfactory stimuli. The fMRI differences shown were synthesized by inverse

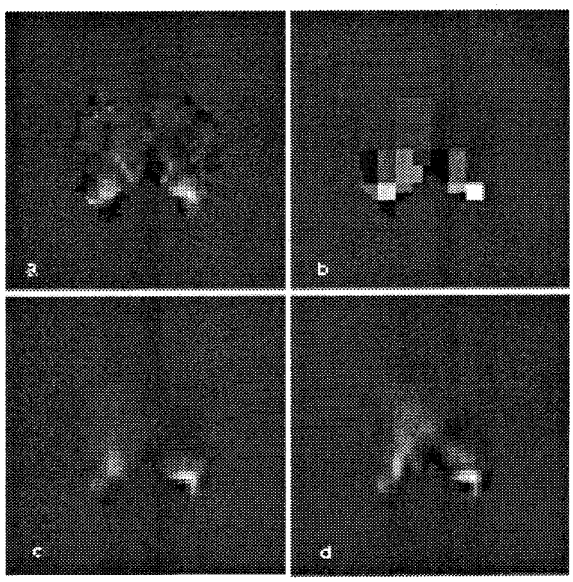

Fig. 2 (a) Average difference image; (b) - (d) resynthesis of (a) from significant wavelet coefficients using zero, first and third order splines.

wavelet transform of significant coefficients only, using cubic spline wavelets.

4. DISCUSSION

The process of globally eliminating nonsignificant resolution channels by (2.13) is analogous to applying a filter to the difference image, which due to the nature of the signal turns out to be essentially a lowpass. However, the important difference from standard lowpass filtering is that the cutoff frequency does not have to be specified beforehand, but is rather determined by statistical testing. This constitutes a flexibility inherent in the method with considerable practical impact, in that it can readily be applied to images acquired on scanners with ill-specified or unknown point-spread functions. Similarly, the testing of the coefficients in significant channels (2.11) can be viewed as a spatially adaptive filtering process, where a specific bandpass filter (the wavelet) is applied at image locations providing significant edge information, while "flat" image regions are smoothed to the extent permitted by the next lower wavelet resolution level. As a result of these implicit filter operations, resynthesis of the difference images based on significant wavelet coefficients only results in smooth, relatively noise-free foci of functional change

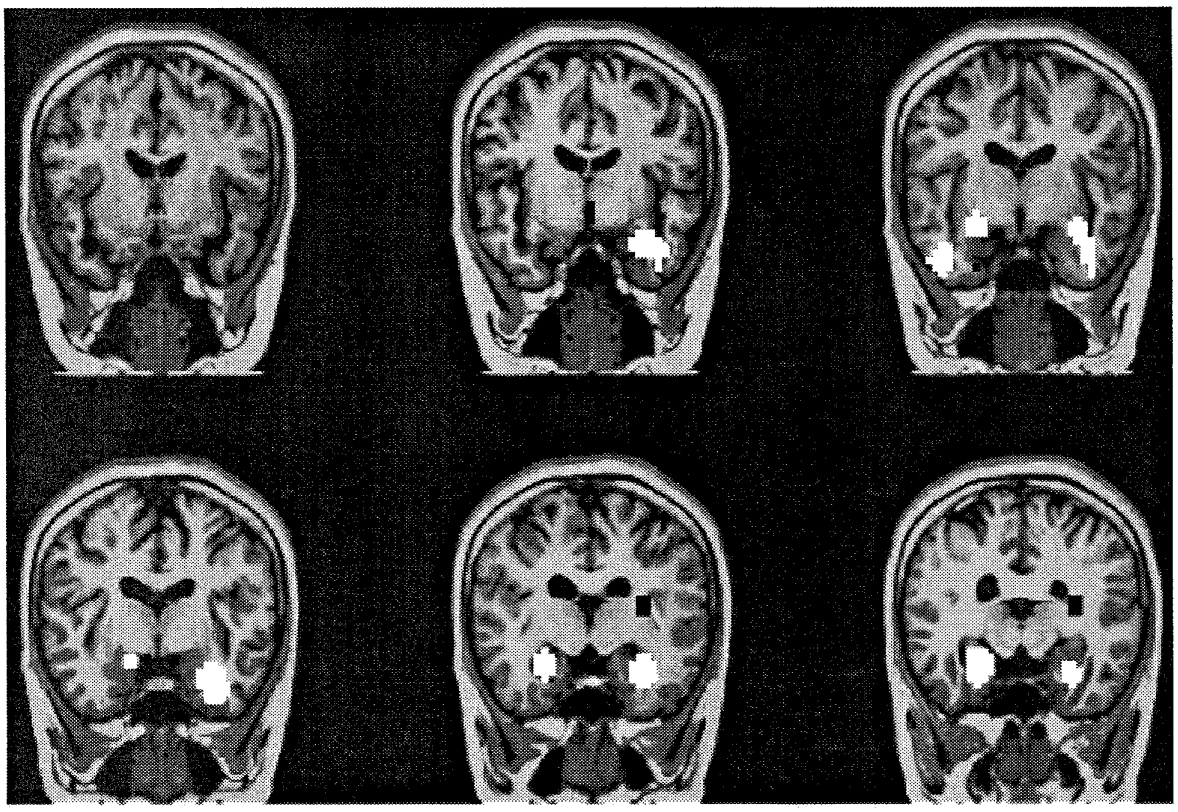

Fig. 3 Contiguous coronal MRI slices (anteroposterior direction from top left to bottom right), tilted at an angle of 45° from postero-superior to antero-inferior. Superimposed are significant functional signal differences >1% due to olfactory stimulation (positive - white, negative - black).

that were not broken up into scattered single-pixel regions by the thresholding employed for the anatomical overlay.

In conclusion, wavelet decomposition permits establishing rigorous significance levels unencumbered by intervoxel correlation. It exploits the higher SNR in low-resolution channels arising from the predominantly lowpass nature of the difference signal to achieve a 10:1 reduction in the number of statistical tests. This results in a lower detection threshold for a given p-level per volume, thereby increasing the sensitivity for localizing biologically relevant signal changes as small as 1%.

REFERENCES

[1] J.W. Prichard, B.R. Rosen, Functional study of the brain by NMR. J Cereb Blood Flow Metab 14:365-372,1994.

[2] J. Duyn, V.S. Mattay, R. Sexton, G. Sobering, F. Barrios, G. Liu, J. Frank, D.R. Weinberger, C.T.W. Moonen., Three-dimensional functional imaging of human brain using echo-shifted FLASH MRI. Magn Reson Med 32:150-155, 1994.

[3] P. Thévenaz, U.E. Ruttimann, M. Unser, Iterative multi-scale registration without landmarks. IEEE ICIP-95, Paper No. 400, 1995.

[4] S.G. Mallat, A theory of multiresolution signal decomposition: the wavelet representation. IEEE Trans Pattern Anal Machine Intell, PAMI-11: 674-693, 1989.

[5] M. Unser, A. Aldroubi, M. Eden, A family of polynomial spline wavelet transforms, Signal Processing 30:141-162, 1993.

[6] U.E. Ruttimann, M. Unser, D. Rio, R.R. Rawlings, The use of the wavelet transform to investigate differences in brain PET images between patients. Proc. SPIE, Vol. 2035, Mathematical Methods in Medical Imaging II:192-203, 1993.